Interaction of Acetone with Single Wall Carbon Nanotubes at Cryogenic Temperatures: A Combined Temperature Programmed Desorption and Theoretical Study

Dmitry Kazachkin,[†,‡] Yoshifumi Nishimura,[§] Stephan Irle,[§,||,⊥] Keiji Morokuma,[||,⊥] Radisav D. Vidic,[#] and Eric Borguet*[,†]

Department of Chemistry, Temple University, Philadelphia, Pennsylvania 19122, Department of Chemical Engineering, University of Pittsburgh, Pittsburgh, Pennsylvania 15261, Department of Chemistry and Institute for Advanced Research, Nagoya University, Nagoya 464-8602, Japan, Fukui Institute for Fundamental Chemistry, Kyoto University, Kyoto 606-8103, Japan, Cherry L. Emerson Center for Scientific Computation and Department of Chemistry, Emory University, Atlanta, Georgia 30322, and Department of Civil and Environmental Engineering, University of Pittsburgh, Pittsburgh, Pennsylvania 15261

Received January 4, 2008. Revised Manuscript Received March 5, 2008

The interaction of acetone with single wall carbon nanotubes (SWCNTs) at low temperatures was studied by a combination of temperature programmed desorption (TPD) and dispersion-augmented density-functional-based tight binding (DFTB-D) theoretical simulations. On the basis of the results of the TPD study and theoretical simulations, the desorption peaks of acetone can be assigned to the following adsorption sites: (i) sites with energy of ∼75 kJ mol^{-1} (T_{des} ∼300 K)—endohedral sites of small diameter nanotubes (∼7.7 Å); (ii) sites with energy 40–68 kJ mol^{-1} (T_{des} ∼240 K)—acetone adsorption on accessible interstitial, groove sites, and endohedral sites of larger nanotubes (∼14 Å); (iii) sites with energy 25–42 kJ mol^{-1} (T_{des} ∼140 K)—acetone adsorption on external walls of SWCNTs and multilayer adsorption. Oxidatively purified SWCNTs have limited access to endohedral sites due to the presence of oxygen functionalities. Oxygen functionalities can be removed by annealing to elevated temperature (900 K) opening access to endohedral sites of nanotubes. Nonpurified, as-received SWCNTs are characterized by limited access for acetone to endohedral sites even after annealing to elevated temperatures (900 K). Annealing of both purified and as-produced SWCNTs to high temperatures (1400 K) leads to reduction of access for acetone molecules to endohedral sites of small nanotubes, probably due to defect self-healing and cap formation at the ends of SWCNTs. No chemical interaction between acetone and SWCNTs was detected for low temperature adsorption experiments. Theoretical simulations of acetone adsorption on finite pristine SWCNTs of different diameters suggest a clear relationship of the adsorption energy with tube sidewall curvature. Adsorption of acetone is due to dispersion forces, with its C−O bond either parallel to the surface or O pointing away from it. No significant charge transfer or polarization was found. Carbon black was used to model amorphous carbonaceous impurities present in as-produced SWCNTs. Desorption of acetone from carbon black revealed two peaks at ∼140 and ∼180–230 K, similar to two acetone desorption peaks from SWCNTs. The characteristic feature of acetone desorption from SWCNTs was peak at ∼300 K that was not observed for carbon black. Care should be taken when assigning TPD peaks for molecules desorbing from carbon nanotubes as amorphous carbon can interfere.

1. Introduction

Carbon materials are of interest for fundamental science and technological applications.[1] After their discovery more then 50 years ago,[2] the importance of carbon nanotubes (CNTs) for technological applications was not initially recognized and became clear only recently.[3,4] The dimensions and properties of CNTs make their application as nanosensors attractive.[5–8]

Acetone is a simple polar organic solvent and a major chemical commodity.[9] Acetone is reported to be the dominant non-methane organic atmospheric pollutant.[10] Moreover, acetone forms in the body during ketogenesis.[11] Thus, there is ongoing interest in the study of the interaction of acetone molecules with CNTs for the development of sensors[6,12–15] to control the environmental release

* Corresponding author. Eric Borguet, Department of Chemistry, Temple University, Philadelphia, PA 19122. Tel: 1-215-204-9696. Fax: 1-215-204-9530. E-mail: eborguet@temple.edu.

† Temple University.

‡ Department of Chemical Engineering, University of Pittsburgh.

§ Nagoya University.

|| Kyoto University.

⊥ Emory University.

Department of Civil and Environmental Engineering, University of Pittsburgh.

(1) Burchell, T. D. *Carbon Materials for Advanced Technologies*; 1999; p 540.

(2) Radushkevich, L. V.; Luk'yanovich, V. M. *Zh. Fiz. Khim.* **1952**, *26*, 88–95.

(3) Iijima, S. *Nature* **1991**, *354*(6348), 56–8.

(4) Tanaka, K.; Yamabe, T.; Fukui, K. *The Science and Technology of Carbon Nanotubes*; Elsevier Science Ltd.: Oxford, 1999; p 191.

(5) Kong, J.; Franklin, N. R.; Zhou, C. W.; Chapline, M. G.; Peng, S.; Cho, K. J.; Dai, H. J. *Science* **2000**, *287*(5453), 622–625.

(6) Robinson, J. A.; Snow, E. S.; Badescu, S. C.; Reinecke, T. L.; Perkins, F. K. *Nano Lett.* **2006**, *6*(8), 1747–1751.

(7) Snow, E. S.; Perkins, F. K.; Houser, E. J.; Badescu, S. C.; Reinecke, T. L. *Science* **2005**, *307*(5717), 1942–1945.

(8) Li, J.; Lu, Y. J.; Ye, Q.; Cinke, M.; Han, J.; Meyyappan, M. *Nano Lett.* **2003**, *3*(7), 929–933.

(9) Kirk, R. E.; Othmer, D. F.; Kroschwitz, J. I. *Kirk-Othmer Concise Encyclopedia of Chemical Technology, 5th Edition*; John Wiley & Sons: New York, 2007.

(10) Singh, H. B.; Ohara, D.; Herlth, D.; Sachse, W.; Blake, D. R.; Bradshaw, J. D.; Kanakidou, M.; Crutzen, P. J. *J. Geophys. Res., [Atmos.]* **1994**, *99*(D1), 1805–19.

(11) VanItallie, T. B.; Nufert, T. H. *Nutr. Rev.* **2003**, *61*(10), 327–341.

(12) Lu, Y.; Partridge, C.; Meyyappan, M.; Li, J. *J. Electroanal. Chem.* **2006**, *593*(1–2), 105–110.

(13) Snow, E. S.; Perkins, F. K. *Nano Lett.* **2005**, *5*(12), 2414–2417.

(14) Parikh, K.; Cattanach, K.; Rao, R.; Suh, D.-S.; Wu, A.; Manohar, S. K. *Sens. Actuators, B: Chem.* **2006**, *B113*(1), 55–63.

10.1021/la800030y CCC: $40.75
Published on Web 07/10/2008

of acetone from industrial sites and to monitor the acetone level in the human body to prevent ketoacidosis, an issue for people with diabetes.[16]

There have been several experimental studies on the interaction of acetone with carbon materials (highly oriented pyrolitic graphite (HOPG) and CNTs) and the application of CNTs to acetone vapor detection.[6,12–15,17–20] Recent publications suggest a chemical interaction of acetone with SWCNTs[19] and multiwall carbon nanotubes (MWCNTs)[20] with a maximum desorption energy of ~100 kJ mol^{-1} and ~68 kJ mol^{-1}, respectively. Chakrapani et al. suggested that the curvature of the CNT surfaces and topological defects play an important role in the strong binding of acetone to the CNT surface.[19] Shih and Li proposed that strong chemical interaction of acetone with MWCNTs is due to topological defects and disorder in MWCNTs.[20] Snow and Perkins used SWCNT-based sensors for acetone detection and proposed that acetone vapors produce a rapid response in the conductance and capacitance of SWCNTs due to charge transfer and polarizability, but did not discuss the adsorption energetics.[13] Later, Robinson et al. reported that defects play an important role in acetone binding to CNTs and the acetone adsorption energy was estimated from conductance curves as a function of acetone pressure to be 41 kJ mol^{-1}, while theoretical calculations for acetone bound to carboxylic groups in proximity to side wall defects gave a binding energy of 34 kJ mol^{-1}.[6] The results of a TPD study on acetone interaction with HOPG suggested that acetone adsorbs in three states: monolayer ($T_{d,max}$ ~165 K), bilayer ($T_{d,max}$ ~155 K), and multilayer ($T_{d,max}$ ~145 K).[17,18] Furthermore, the presence of oxygen functionalities has been shown to influence the interaction of acetone with HOPG.[18] Here, we present the results of a temperature programmed desorption (TPD) investigation and theoretical simulations of acetone adsorption on SWCNTs at cryogenic temperatures, and explore the influence of oxygen functionalities and annealing temperature on acetone adsorption on SWCNTs. We discuss the implications of these results on SWCNT-based sensor operation and SWCNT thermal processing.

2. Experimental and Theoretical Approach

2.1. Materials. As-produced (nonpurified) SWCNTs, synthesized by the HiPco[21] method, were purchased from CNI (Houston, TX). To remove the residual catalysts (Fe) and amorphous carbon, a two-step purification procedure was used.[22,23] First, nonpurified SWCNTs were placed in a plug−flow reactor made of a Pyrex U-tube and treated at 250 °C for 5 h in a flow of prepurified air (Airgas) saturated with water vapor, prepared by bubbling room temperature air through ultrapure water (Easypure II, Barnstead). Second, the oxidized SWCNTs were transferred to a flask and sonicated for 3 h in 6 M HCl (Fisher Scientific) using a laboratory ultrasonic bath (Bransonic 2200). The solution containing SWCNTs was filtered using a 2 μm filter (Whatman). The sample on the filter was rinsed with 6 M HCl and then ultrapure water to wash out HCl until pH neutrality was reached. The filter was then dried at 60 °C for 12 h in ambient air. The yield of purified SWCNTs was evaluated to be ~6–9 wt %.

The purity of SWCNTs after air/HCl treatment was checked with X-ray photoelectron spectroscopy and thermogravimetric analysis (TGA). No XPS signal, above the noise level, from Fe was detected in the purified SWCNTs, suggesting an iron content of less than 5 wt % (detection limit for conditions used), whereas the as-produced SWCNTs gave a distinct doublet from Fe (Supporting Information Figure S1). Typically, air/HCl purification reduces residual iron content from initial 20–30 wt % to 1–5 wt % according to TGA (Supporting Information Figure S1).[23,24]

Before introduction into the UHV chamber, the samples were sonicated in acetone (Fisher, ACS grade) for 1 h and then deposited by drop-and-dry method onto a W-grid (Alfa Aesar, 100 mesh, 0.002 in wire diameter) in a flow of preheated air (~330 K).

2.2. Experimental Setup. Temperature programmed desorption experiments with mass spectroscopy monitoring (TPD-MS) were performed in a stainless steel ultrahigh vacuum chamber, described in detail earlier,[25] with a base pressure of less than 5×10^{-9} Torr. Before sample deposition, the W-grid was attached by nickel clamps to the sample holder copper wires of a vacuum electrical feedthrough attached to the bottom of a dewar. A K-type thermocouple (Omega) with a short time response was spot-welded to the W-grid. The design of the sample holder allows cooling of the sample to cryogenic temperatures (<100 K) and resistive heating to 1400 K.

Acetone vapor (~10^{-7}−10^{-6} Torr) was dosed through a leak valve (Varian) into the vacuum chamber to a fixed pressure for the time required to achieve the desired dose (Note: exposures are given in Langmuir units, 1 L = 10^{-6} Torr s). Uncorrected pressure was monitored with a nude ion gauge (Varian). To heat the sample, direct current from a power supply (Kepco) was driven through the W-grid and the temperature was monitored via the thermocouple. A shielded residual gas analyzer (AccuQuad RGA 300, Stanford Research Systems) was used to monitor the desorbing species. Custom programs written in *Labview* were used to control the temperature, monitor the dosing, and record TPD-MS spectra.

2.3. Sample Pretreatment and Gas Exposure Procedures. The SWCNTs sample was placed in a vacuum chamber and evacuated to $<5 \times 10^{-9}$ Torr. When the sample was cooled to 90–100 K, the resulting base pressure was $<1 \times 10^{-9}$ Torr. Then, the sample was heated at 2 K s^{-1} to 500 K and held at 500 K for 2 h under vacuum to remove residual solvent and adsorbed gases (this sample will be referred to as SWCNTs-500). After 2 h at 500 K, temperature was quenched back to 90–100 K. The SWCNTs-500 was cooled to 100 K and the desired amount of acetone was dosed to the sample. After dosing, the pressure was allowed to reach approximately the same level as before dosing and allowed to stabilize for 2–5 min. Only after that were TPD-MS spectra collected. The following doses of acetone were used: 1, 5, 10, 25, 50, 100, 500, and 1000 L. After the last dose of acetone was injected and TPD-MS was collected, the sample was allowed to warm up to ambient temperature.

On the next day, the sample was annealed to a higher temperature. The anneal temperatures (and times) used were 700 K (1 h), 900 K (0.5 h), and 1400 K (5 min). To indicate the anneal temperature of the sample used before acetone adsorption, we abbreviated the corresponding samples as SWCNTs-500, SWCNTs-700, SWCNTs-900, and SWCNTs-1400. The adsorption energies that were evaluated from TPD profiles were calculated on the basis of Redhead analysis with the assumption of a pre-exponential factor of 10^{13} s^{-1}.[26]

2.4. Theoretical Studies−Computational Methodology. Similar to our approach in a previous study,[27] we have first compared the performance of the dispersion-augmented self-consistent-charge

(15) Guirado-Lopez, R. A.; Sanchez, M.; Rincon, M. E. *J. Phys. Chem. C* **2007**, *111*(1), 57–65.
(16) Federici, M. O.; Benedetti, M. M. *Diabetes Res. Clin. Practice* **2006**, *74*(Supplement 2), S77–S81.
(17) Kwon, S.; Russell, J.; Zhao, X.; Vidic, R. D.; Johnson, J. K.; Borguet, E. *Langmuir* **2002**, *18*(7), 2595–2600.
(18) Kwon, S.; Vidic, R.; Borguet, E. *Surf. Sci.* **2003**, *522*(1–3), 17–26.
(19) Chakrapani, N.; Zhang, Y. M.; Nayak, S. K.; Moore, J. A.; Carroll, D. L.; Choi, Y. Y.; Ajayan, P. M. *J. Phys. Chem. B* **2003**, *107*(35), 9308–9311.
(20) Shih, Y.-h.; Li, M.-s. *J. Hazardous Mater.* **2008**, *154* (1−3), 21−28.
(21) Nikolaev, P.; Bronikowski, M. J.; Bradley, R. K.; Rohmund, F.; Colbert, D. T.; Smith, K. A.; Smalley, R. E. *Chem. Phys. Lett.* **1999**, *313*(1–2), 91–97.
(22) Chiang, I. W.; Brinson, B. E.; Smalley, R. E.; Margrave, J. L.; Hauge, R. H. *J. Phys. Chem. B* **2001**, *105*(6), 1157–1161.
(23) Chiang, I. W.; Brinson, B. E.; Huang, A. Y.; Willis, P. A.; Bronikowski, M. J.; Margrave, J. L.; Smalley, R. E.; Hauge, R. H. *J. Phys. Chem. B* **2001**, *105*(35), 8297–8301.
(24) Feng, X.; Matranga, C.; Vidic, R.; Borguet, E. *J. Phys. Chem. B* **2004**, *108*(52), 19949–19954.
(25) Kwon, S.; Borguet, E.; Vidic, R. D. *Environ. Sci. Technol.* **2002**, *36*(19), 4162–4169.
(26) Redhead, P. A. *Vacuum* **1962**, *12*, 203–11.
(27) Feng, X.; Irle, S.; Witek, H.; Morokuma, K.; Vidic, R.; Borguet, E. *J. Am. Chem. Soc.* **2005**, *127*(30), 10533–10538.

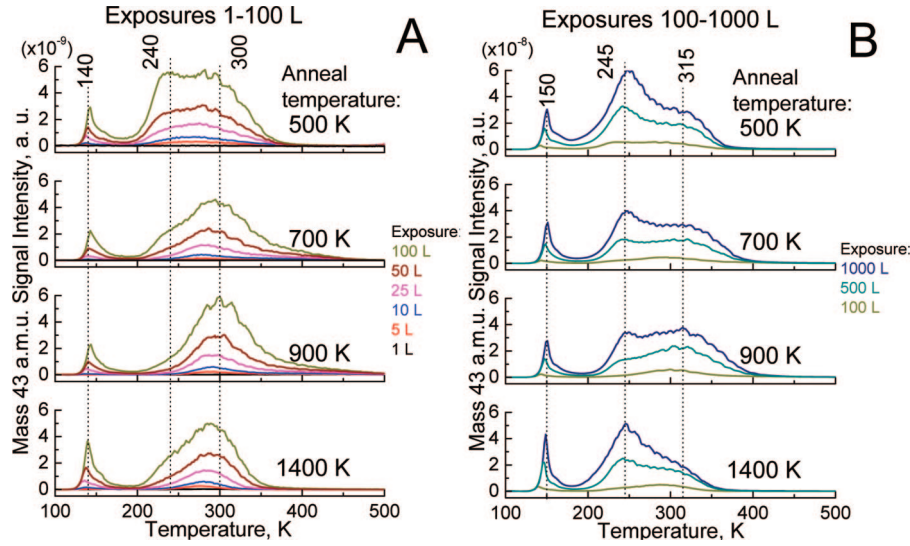

Figure 1. Desorption of acetone (mass 43 amu (e.g., CH_3CO)) from purified SWCNTs annealed to 500, 700, 900, and 1400 K. (A) Acetone exposure 1−100 L. (B) Acetone exposure 100−1000 L. Sites with three different adsorption energies ~35, 50, and 75 kJ mol^{-1} appear to be present on SWCNTs. The acetone uptake by each site depends on SWCNT anneal temperature.

density functional tight binding[28,29] (SCC-DFTB-D, denoted in the following DFTB-D for brevity) method for the prediction of Cπ-acetone interaction energies ΔE to the corresponding *ab initio* large-basis-set MP2 energetics for a coronene ($C_{24}H_{12}$)−acetone model system. Here, we employed the resolution-of-identity (RI-) approach for the MP2 calculations as implemented in the program system TURBOMOLE,[30] using the supplied Ahlrichs basis sets SVP (split-valence polarized, containing up to d/p basis functions for second and first row elements),[31] TZVPP (triplet-ζ valence polarized, containing up to f/d basis functions for second and first row elements),[32] and QZVPP (quadruple-ζ polarized, containing up to g/d basis functions for second and first row elements),[33] and their corresponding auxiliary basis sets for the RI approximation.[30] Full geometry optimizations for various molecular adsorption configurations of the acetone molecule relative to the coronene plane were performed at the MP2/SVP levels of theory as well as at the SCC-DFTB-D level for comparison, making use of molecular symmetry where possible for MP2 calculations. MP2/TZVPP and MP2/QZVPP single point energies were computed for the MP2/SVP geometries. The influence of the basis set superposition error (BSSE) on ΔE was evaluated by performing standard Boys–Bernardi counterpoise correction.[34] In all calculations, default convergence criteria were adapted for wave functions and geometries. The DFTB-D method includes the dispersion energy E_{dis} by adding the sum of a two-center London dispersion term between nuclei α and β separated from each other by a distance $R_{\alpha\beta}$

$$E_{dis} = -\sum_{\alpha\beta} f(R_{\alpha\beta}) C_6^{\alpha\beta} (R_{\alpha\beta})^{-6},$$
$$f(R_{\alpha,\beta}) = [1-\exp(-3*(R_{\alpha,\beta}/R_0)^7)]^4 \quad (1)$$

where $f(R_{\alpha\beta})$ is a damping function to suppress contributions of E_{dis} for small interatomic distances where the London dispersion term is not valid. We follow Elstner et al. who assume R_0 to be 3.8 Å for all elements of the first row of the periodic table.[28] The derivation of the C_6 parameters was described in detail elsewhere.[28] Recent, very favorable performance benchmarks were described for instance for carbon nanosystems[35–37] and biosystems.[38]

3. Experimental Results

The desorption of acetone was followed by monitoring the 43 amu (CH_3CO) and 58 amu ($CH_3(CO)CH_3$) signals. Our data will be presented in terms of 43 amu profile as it was the dominant fragment in the mass spectrum of acetone vapors: the signal for the parent fragment 58 amu was 4.2 times less intense than the 43 amu signal. In addition, TPD-MS for masses 44 and 18 amu were recorded.

Acetone desorption from purified SWCNTs was characterized by three desorption peaks in the 1–100 L exposure range (Figure 1A). For SWCNTs-500, two dominant peaks were present at ~240 (~50 kJ mol^{-1}) and ~300 K (~75 kJ mol^{-1}), and a smaller peak at 140 K (~35 kJ mol^{-1}). The peak at 300 K grew faster than the other peaks for exposures of 1–50 L (Figure 1A), while for higher exposures (>50 L), the peak at 240 K for SWCNTs-500 increased faster than the peak at 300 K. For samples annealed to higher temperatures, the ratio between 240 and 300 K peaks changed: for the SWCNTs-700 and SWCNTs-900 samples, the peak at 300 K was dominant for exposures up to 100 L (Figure 1A), suggesting limited access to sites with the highest adsorption energy for SWCNTs-500. The annealing to 1400 K decreased the 300 K peak intensity at the expense of the 140 and 240 K peaks, reversing the tendency observed for 500–700–900 K annealing temperatures, i.e., the increase of intensity for the 300 K peak. The comparison of acetone desorption profiles for SWCNTs-900 and SWCNTs-1400 suggests the loss of or limited accessibility to the sites responsible for the peak at 300 K for SWCNTs-1400 in comparison with SWCNTs-900 (Figure 1A) at the expense of sites responsible for the peaks at 140 and 240

(28) Elstner, M.; Hobza, P.; Frauenheim, T.; Suhai, S.; Kaxiras, E. *J. Chem. Phys.* **2001**, *114*, 5149–5155.
(29) Elstner, M.; Porezag, D.; Jungnickel, G.; Elsner, J.; Haugk, M.; Frauenheim, T.; Suhai, S.; Seifert, G. *Phys. Rev. B* **1998**, *58*, 7260–7268.
(30) Weigend, F.; Koehn, A.; Haettig, S. *J. Chem. Phys.* **2002**, *116*(8), 3175–3183.
(31) Schäfer, A.; Horn, H.; Ahlrichs, R. *J. Chem. Phys.* **1992**, *97*(4), 2571–2577.
(32) Schäfer, A.; Huber, C.; Ahlrichs, R. *J. Chem. Phys.* **1994**, *100*(8), 5829–5835.
(33) Weigend, F.; Furche, F.; Ahlrichs, R. *J. Chem. Phys.* **2003**, *119*, 12753–12762.
(34) Boys, S. F.; Bernardi, F. *Mol. Phys.* **1970**, *19*(4), 553–566.
(35) Lin, C. S.; Zhang, R. Q.; Lee, S. T.; Elstner, M.; Frauenheim, T.; Wan, L. J. *J. Phys. Chem. B* **2005**, *109*, 14183–14188.
(36) Pankewitz, T.; Klopper, W. *J. Phys. Chem. C* **2007**, *111*(51), 18917–18926.
(37) Zhechkov, L.; Heine, T.; Patchkovskii, S.; Seifert, G.; Duarte, H. A. *J. Chem. Theor. Comput.* **2005**, *1*(5), 841–847.
(38) Kubar, T.; Hanus, M.; Ryjacek, F.; Hobza, P. *Chem.—Eur. J.* **2006**, *12*, 280–290.

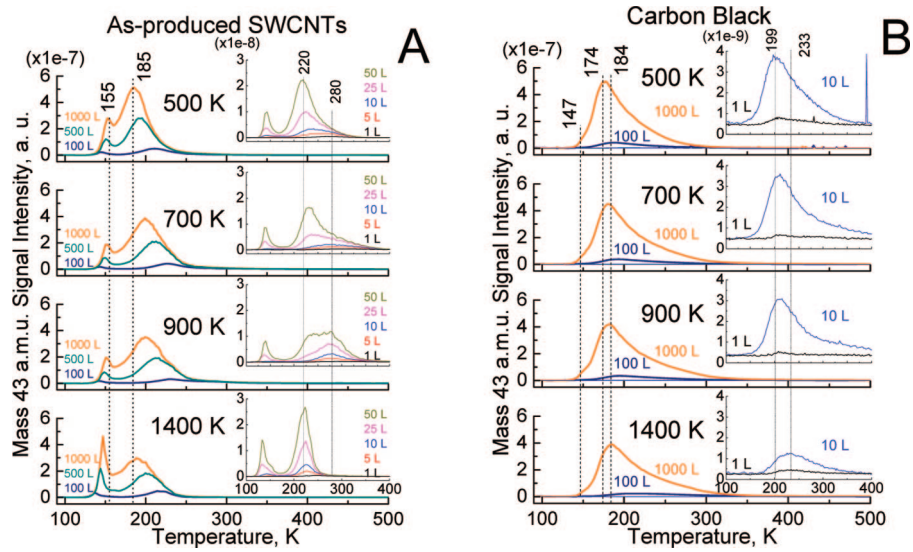

Figure 2. Comparison of acetone adsorption on as-produced SWCNTs (A) and carbon black (B) annealed to different temperatures. As produced SWCNTs contain amorphous carbon, iron catalyst, and are characterized by low access to the endohedral sites due to caps present at the ends of SWCNTs.[39,40] Three desorption peaks of acetone for as-produced SWCNTs can be detected: 140–150, 180–240, and 280 K. As-received carbon black has a limited porous structure that favors stronger acetone adsorption than HOPG.[17,19] Two desorption peaks can be detected for carbon black: small shoulder at 140–150 K and intense peak at 180–240 K.

K. Qualitatively, the acetone desorption profile for SWCNTs-1400 looked similar to the profile for SWCNTs-700, except for the absence of the high temperature tail that lasts up to 450 K for the SWCNTs-700 sample. The SWCNT anneal temperature had a strong impact on the acetone adsorption behavior. It appears that annealing to consecutively higher temperatures (500–700–900 K) opened access to energetically more favorable adsorption sites (i.e., peak at 300 K and extended up to 450 K desorption tail), while annealing to 1400 K led to partial reblocking of these sites.

To understand whether acetone undergoes irreversible chemical transformation during interaction with SWCNTs,[19,20] several acetone fragments were recorded simultaneously during TPD: 43 amu (CH_3CO), 15 amu (CH_3), 58 amu ($CH_3C(O)CH_3$), and 28 amu (CO). The desorption profiles of all acetone fragments are similar (Supporting Information Figure S3). Moreover, the relative intensities of the different mass fragments were the same as for gas-phase acetone (the relative intensities of the different mass fragments for gas-phase acetone were obtained by introducing a constant presure of acetone (10^{-7} Torr) into the TPD chamber while monitoring the mass spectrum (1−100 amu). Those findings imply that acetone cryogenically adsorbed on SWCNTs desorbs as an intact molecule.

Several control experiments were performed to verify the assignment of TPD-MS peaks. First, the interaction of acetone with the W-grid, used as a sample support, was studied as a function of the anneal temperature: independent of anneal temperature acetone desorbs from the W-grid with a maximum at 136–153 K depending on acetone exposure (5–1000 L) (Supporting Information Figure S2).

A second control experiment was the adsorption of acetone on as-produced SWCNTs without any chemical purification treatment (Figure 2A). The as-produced SWCNTs are characterized by admixtures of amorphous carbon and iron catalyst particles[21] that might influence the adsorption behavior of the purified SWCNTs as well. Control experiments identified three peaks for acetone desorption from the as-produced SWCNTs: 140–150, 180–240, and 280 K. The peak at 280 K had a small intensity and was observed as a shoulder of the more intense peak at 220–240 K at moderate exposures (<100 L). Only after anneal at 900 K did the peak at 280 K became comparable in intensity to the peak at 220–240 K (≤50 L). Annealing of the as-produced SWCNTs to 1400 K resulted in a compete cancellation of the 280 K peak. High acetone exposures (1000 L) to the as-produced SWCNTs resulted in a broad peak with desorption maximum at 185–200 K depending on anneal temperature (Figure 2A). To summarize, as-produced SWCNTs had peaks similar to purified SWCNTs except that the ratio between peaks was different. The peak at 180–240 K was the dominant feature in desorption spectra of acetone for the as-produced SWCNTs, while the peak at 280 K was pronounced only for low exposures (<50 L), and much smaller for purified SWCNTs.

In order to isolate features characteristic of acetone interaction with SWCNTs, acetone adsorption was performed on a carbon black sample (CB-460, Cabot) characterized by a limited porous structure ($S_{BET} \sim 76$ m^2/g). Carbon black was used as a model material for amorphous carbon present in as-produced SWCNTs. Carbon black was degassed at the same temperatures as SWCNTs before acetone dosing (Figure 2B). For the carbon black sample annealed to 500 K, a peak with desorption maximum at 200 K was observed for low exposures (10 L) that shifted to lower temperatures with exposure increase: for the dose of 1000 L peak shifted to 174 K (Figure 2B). The small shoulder at 150 K was noticeable only for high acetone exposures. Annealing to consecutively higher temperatures resulted in a shift of the acetone (10 L) desorption peak maxima from 199 K (anneal 500 K) to 233 K (anneal 1400 K). Overall, acetone adsorption on carbon black was characterized by two peaks: the peak at 150 K noticeable only for high exposures and the peak at 180−240 K. The position of 180−240 K peak was a function of exposure (the higher exposure - the lower $T_{des.}$) and anneal temperature (the higher anneal temperature - the higher $T_{des.}$) (Figure 2B). Acetone adsorption behavior on the carbon black at high exposures (1000 L) annealed at 500−700−900 K was similar to the behavior of acetone adsorption on as-produced SWCNTs annealed to the same temperatures suggesting that the acetone adsorption behavior

(39) Ajayan, P. M.; Ebbesen, T. W. *Rep. Prog. Phys.* **1997**, *60*(10), 1025–1062.

(40) Dresselhaus, M. S.; Dresselhaus, G.; Eklund, P. C., *Science of Fullerenes and Carbon Nanotubes*; Academic Press: London, 1996.

of as-produced SWCNTs was, in some extent, determined by the presence of carbonaceous impurities. The acetone desorption peak at 280−300 K, specific for as-produced and purified SWCNTs, was absent for carbon black.

4. Discussion of Experimental Results

Previous experiments suggest that CNT purification by oxidative methods leads to the introduction of oxygen functionalities[24,27,41,42] and defects[43,44] to SWCNTs. Typically, nanotubes assemble into bundles[45] due to van der Waals forces.[46] The bundle structure favors multiple adsorption sites such as endohedral, interstitial, grooves, and external walls. It is reasonable to expect different interaction energies for molecules adsorbed on different sites.

The observation of all adsorption sites is possible if all the sites are accessible. The interstitial sites of nanotubes (with $d \sim 10$ Å) bundles are ∼0.26 nm[47] wide and cannot be filled even by small molecules, e.g., Xe, CH_4, Ne,[48] and Ar.[49] On the other hand, interstitial sites of heterogeneous bundles, formed by nanotubes of different diameters, are accessible as was shown by Monte Carlo simulations.[50] A narrow distribution of nanotube diameters is also important for the observation of distinct desorption peaks as the adsorption of acetone on endohedral sites becomes stronger with increasing SWCNT wall curvature (see Figure 5).

Adsorption energies depend also on intermolecular interactions. For alkanes adsorbed on bundled SWCNTs, the existence of three adsorption sites has been suggested, endohedral, grooves, and external walls, while the fourth observed TPD peak was assigned to multilayer adsorption.[51] In contrast to the well-resolved desorption peaks of paraffins,[51] methanol (CH_3OH) adsorption on SWCNTs was characterized by a single peak ∼150 K with a weak high temperature shoulder that was noticeable only for small exposures.[52] The absence of distinct peaks corresponding to different adsorption sites for methanol suggests that intermolecular interactions (e.g., hydrogen bonding) might be important for methanol.[52] There is no evidence that acetone−acetone interactions are responsible for the observed desorption behavior (Figure 1). The desorption of acetone multilayers, reflecting intermolecular interactions, from the surface of HOPG occurs at ∼145 K.[17]

In order to assign the desorption peaks of acetone from SWCNTs observed in the TPD spectra, we considered four adsorption sites: endohedral, interstitial (including large interstitial channels[50]), grooves, and external walls. The TPD spectra, however, show only three desorption peaks (Figure 1). For as-produced SWCNTs, characterized by capped ends,[39,40] the intensity of the desorption peak at 300 K was suppressed, while peaks at 140 and 240 K were well-developed (Figure 2A). Finally, peaks with desorption temperatures higher than 180 K, observed for acetone adsorption on SWCNTs, were not observed for acetone adsorption on HOPG.[17,18]

On the basis of the preceding discussion and the results of theoretical simulations (section 5), the following assignments were made: the peak at ∼300 K (with estimated adsorption energy of ∼75 kJ mol^{-1}) was assigned to the adsorption of acetone on endohedral sites of small SWCNTs (∼7.7 Å). The peak at ∼300 K had a limited intensity for oxidatively purified SWCNTs-500 (Figure 1) and for the as-produced SWCNTs (Figure 2A), both known to have limited access to the endohedral sites.[39,40,53] The peak at ∼240 K (∼50 kJ mol^{-1}) was assigned to adsorption of acetone on grooves, in accessible interstitial channels, and in endohedral sites of large SWCNTs (∼14 Å). The peak at 240 K could arise from acetone interaction with amorphous carbon, as it has been shown to be present for carbon black (Figure 2B). Finally, the peak at 140 K (∼30 kJ mol^{-1}) was assigned to acetone adsorption on external walls and multilayer adsorption.[17,18] Desorption of acetone from the W-grid could also contribute to the 140 K peak signal intensity (Supporting Information Figure S2).

Accessibility of endohedral sites appears to be strongly affected by the pretreatment procedure. Endohedral sites of small diameter (∼7.7 Å) oxidatively purified SWCNTs are presumably blocked by oxygen functionalities (Figure 3A).[24] These are probably not removed until annealing to ≥600 K, when some surface functional groups decompose, [24] allowing more access to endohedral sites (Supporting Information Figure S4). Annealing of SWCNTs to 900 K results in some additional decomposition of oxygen functionalities in agreement with the TPD profile of CO_2 release (Supporting Information Figure S4), further increasing access to endohedral sites (Figure 3B),[24,53] The acetone TPD profiles of the SWCNTs samples annealed to 700 and 900 K are characterized by temperature tails that extend up to 450 K, associated with an apparent acetone desorption energies ∼110 kJ mol^{-1}. We believe that nanotubes of small diameter (<0.9 nm) might contribute to such an extended desorption profile due to high binding potential or/and diffusion limitations. To summarize, the presence of oxygen functionalities, which form on SWCNTs during the oxidative purification process, limits acetone access to endohedral sites, until removal by annealing to high temperatures (700–900 K) in agreement with the literature.[53]

We think that, after anneal of SWCNTs to 1400 K, the nanotubes become partially closed and less defective due self-healing that reduces access to endohedral sites: the desorption peak at ∼300 K was reduced in intensity for SWCNTs after anneal at 1400 K (Figures 1 and 2A). It was shown by molecular dynamics simulations that CNT defects may disappear by recombination with carbon adatoms and by Stone-Wales defects formation.[54] Moreover, according to results of theoretical calculations, pristine nanotubes can cap themselves at elevated temperatures.[55] It was established by HR-TEM that anneal of SWCNTs even to 1073 K leads to partial closing of SWCNTs.[56]

(41) Kuznetsova, A.; Popova, I.; Yates, J. T., Jr.; Bronikowski, M. J.; Huffman, C. B.; Liu, J.; Smalley, R. E.; Hwu, H. H. Chen, J. G. *J. Am. Chem. Soc.* 2001, *123* (43), 10699–10704.

(42) Yang, C. M.; Kanoh, H.; Kaneko, K.; Yudasaka, M.; Iijima, S. *J. Phys. Chem. B* 2002, *106* (35), 8994–8999.

(43) Martinez, M. T.; Callejas, M. A.; Benito, A. M.; Cochet, M.; Seeger, T.; Anson, A.; Schreiber, J.; Gordon, C.; Marhic, C.; Chauvet, O.; Maser, W. K. *Nanotechnology* 2003, *14* (7), 691–695.

(44) Martinez, M. T.; Callejas, M. A.; Benito, A. M.; Cochet, M.; Seeger, T.; Anson, A.; Schreiber, J.; Gordon, C.; Marhic, C.; Chauvet, O.; Fierro, J. L. G.; Maser, W. K. *Carbon* 2003, *41* (12), 2247–2256.

(45) Thess, A.; Lee, R.; Nikolaev, P.; Dai, H.; Petit, P.; Robert, J.; Xu, C.; Lee, Y. H.; Kim, S. G.; Rinzler, A. G.; Colbert, D. T.; Scuseria, G. E.; Tomanek, D.; Fischer, J. E.; Smalley, R. E. *Science (Washington, D. C.)* 1996, *273* (5274), 483–487.

(46) Girifalco, L. A.; Hodak, M.; Lee, R. S. *Phys. Rev. B* 2000, *62* (19), 13104–13110.

(47) Maniwa, Y.; Kataura, H.; Abe, M.; Suzuki, S.; Achiba, Y.; Kira, H.; Matsuda, K. *J. Phys. Soc. Jpn.* **2002**, *71*(12), 2863–2866.

(48) Talapatra, S.; Zambano, A. Z.; Weber, S. E.; Migone, A. D. *Phys. Rev. Lett.* **2000**, *85*(1), 138.

(49) Rols, S.; Johnson, M. R.; Zeppenfeld, P.; Bienfait, M.; Vilches, O. E.; Schneble, J. *Phys. Rev. B* **2005**, *71*(15), 155411.

(50) Shi, W.; Johnson, J. K. *Phys. Rev. Lett.* **2003**, *91*(1), 015504.

(51) Kondratyuk, P.; Yates, J. *Acc. Chem. Res.* 2007.

(52) Burghaus, U.; Bye, D.; Cosert, K.; Goering, J.; Guerard, A.; Kadossov, E.; Lee, E.; Nadoyama, Y.; Richter, N.; Schaefer, E.; Smith, J.; Ulness, D.; Wymore, B. *Chem. Phys. Lett.* **2007**, *442*(4–6), 344–347.

(53) Kuznetsova, A.; Mawhinney, D. B.; Naumenko, V.; Yates, J. T.; Liu, J.; Smalley, R. E. *Chem. Phys. Lett.* **2000**, *321*(3,4), 292–296.

(54) Krasheninnikov, A. V.; Nordlund, K.; Keinonen, J. *Phys. Rev. B* **2002**, *65*(16), 165423.

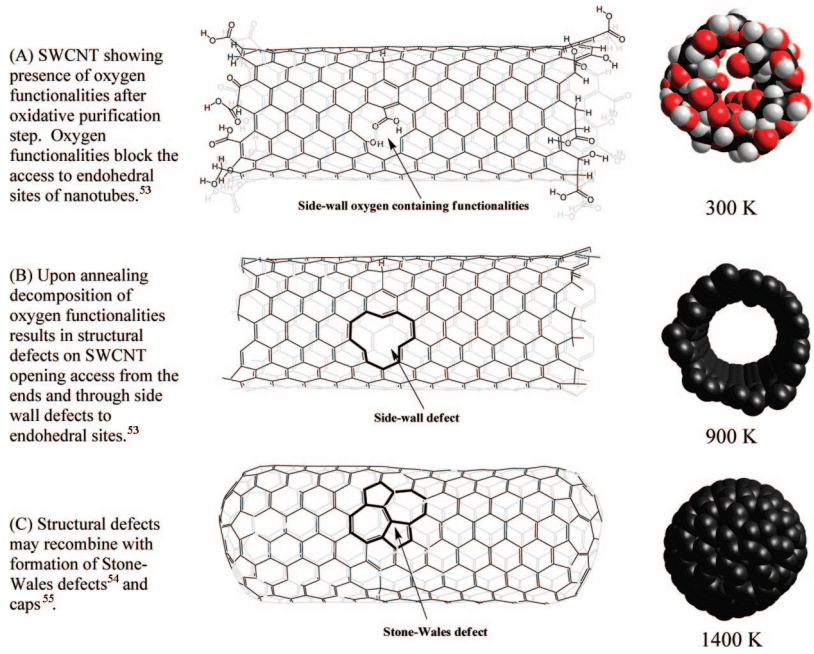

Figure 3. Proposed evolution of endohedral sites accessibility based on SWCNTs (8,8) model. Color code: black, carbon; red, oxygen; white, hydrogen.

Reduction of sidewall defects and closing of nanotubes limit the accessibility of endohedral sites (Figure 3C). Another possible explanation for the disappearance of the acetone peak at 300 K is a temperature-induced coalescence of SWCNTs with formation of nanotubes of larger diameter.[57,58] We believe that coalescence of nanotubes is not likely in our work, because the conditions used (1400 K) are milder than conditions ($\geq$1773 K) where coalescence of SWCNTs was reported.[57,58] Moreover, Raman data suggest that SWCNTs preserve their tubular structure even after annealing to 1300/1400 K.[24]

The results on cryogenic adsorption of acetone on SWCNTs suggest the presence of adsorption sites that are not characteristic for acetone adsorption on a simple planar carbon surface, e.g., HOPG.[17,18] Moreover, the C-black sample studied for control purposes showed two desorption peaks at 140–150 K and a peak at 200–230 K (Figure 2B). It appears that the acetone binding energy correlates with available porous structure: adsorption in pores is defined by dispersion forces and ultimately the ratio of the molecule size to the pore diameter defines the overall potential.[59,60] For pores with a large diameter, i.e., significantly exceeding the effective size of an adsorbate, the interaction potential would be close to the potential of a flat surface (e.g., HOPG). As the diameter of the pore reduces, the adsorbate will interact more strongly with the internal walls (see section 5). The differences in adsorption behavior among HOPG, carbon black, and SWCNTs are likely associated with the morphology of each material. HOPG is known to have no porous structure,[61] while carbon black has limited porous structure. SWCNTs have unique adsorption properties due to self-organization in bundles that provides a variety of adsorption sites, whose availability depends on pretreatment conditions. The increased capacity for acetone strongly bound to the SWCNTs after purification correlates well with an increase of microporous structure.[62,63]

We detected no irreversible chemical interaction upon low temperature adsorption of acetone on SWCNTs (Supporting Information Figure S3). It has been suggested that acetone adsorbs chemically on as-produced SWCNTs[19] and MWCNTs.[20] The conditions under which acetone was introduced to SWCNTs in the present work (100 K, 10^{-6} Torr) are different from the conditions used by others.[19,20] Chakrapani et al. used sonication to interact SWCNTs with acetone.[19] It is possible that sonication-induced changes in temperature and pressure[64] might result in chemical interaction of acetone with SWCNTs.[19] Shih and Li, who dosed acetone to MWCNTs at temperatures of $\geq$303 K, proposed chemical interaction between MWCNTs and acetone based on high adsorption enthalpies (-68.3 kJ mol^{-1}), but provided no further evidence.[20] The highest estimated adsorption energy for acetone adsorbed on SWCNTs-700 and 900 was $\sim$110 kJ mol^{-1} (450 K tail). However, our results suggest that acetone dosed from the gas phase desorbs as an intact molecule, suggesting that the interaction of acetone with SWCNTs upon low temperature adsorption is chemically reversible.

The results of the current work do not provide insight into why SWCNT-based sensors respond to acetone vapors.[6,13] Acetone adsorbed at low temperature interacts reversibly with SWCNTs due to dispersion forces with essentially no electron transfer or polarization (section 5). Charge transfer might occur for acetone adsorption on oxygen functionalities, as it was established that sensor response improved with increasing degree of SWCNT oxidation.[6] It should be noted that the interaction of

(55) Zheng, G.; Irle, S.; Elstner, M.; Morokuma, K. *J. Phys. Chem. A* **2004**, *108*(15), 3182–3194.
(56) Geng, H. Z.; Zhang, X. B.; Mao, S. H.; Kleinhammes, A.; Shimoda, H.; Wu, Y.; Zhou, O. *Chem. Phys. Lett.* **2004**, *399*(1–3), 109–113.
(57) Fang, S. L.; Rao, A. M.; Eklund, P. C.; Nikolaev, P.; Rinzler, A. G.; Smalley, R. E. *J. Mater. Res.* **1998**, *13*(9), 2405–2411.
(58) Kim, U. J.; Gutierrez, H. R.; Kim, J. P.; Eklund, P. C. *J. Phys. Chem. B* **2005**, *109*(49), 23358–23365.
(59) Do, D. D. *Adsorption Analysis: Equilibria and Kinetics*; Imperial College Press: London, 1998.
(60) Gregg, S. J.; Sing, K. S., *Adsorption, Surface Area, and Porosity*, 2nd ed.; Academic Press: London, 1982.
(61) Pierson, H. O., *Handbook of carbon, graphite, diamond, and fullerenes*; Noyes Publications: Park Ridge, NJ, 1993.
(62) Yang, C.-M.; Kaneko, K.; Yudasaka, M.; Iijima, S. *Phys. B: Condens. Matter* **2002**, *323*(1–4), 140–142.
(63) Yang, C. M.; Kaneko, K.; Yudasaka, M.; Iijima, S. *Nano Lett.* **2002**, *2*(4), 385–388.
(64) Suslick, K. S. *Science* **1990**, *247*(4949, Pt. 1), 1439–45.

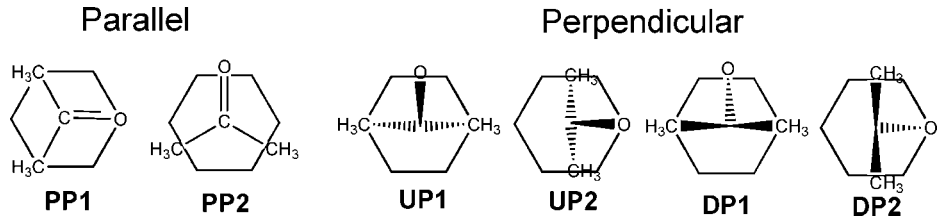

Figure 4. Relative orientations of the acetone molecule on the central hexagon ring of coronene. Only the central coronene ring is shown, and is positioned underneath the acetone molecule. From left to right: planar parallel 1 (**PP1**) and 2 (**PP2**), up-perpendicular 1 (**UP1**) and 2 (**UP2**), and down-perpendicular 1 (**DP1**) and 2 (**DP2**).

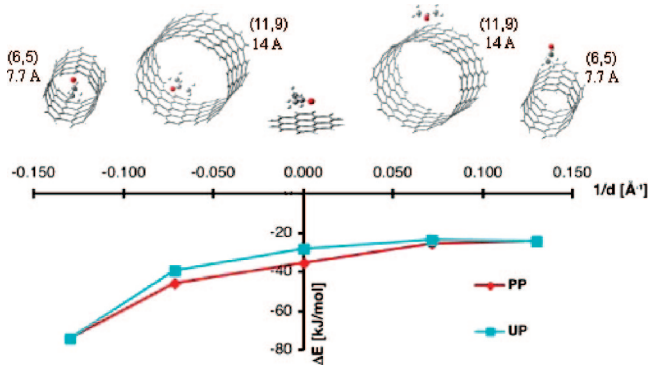

Figure 5. DFTB-D interaction energy ΔE plotted versus sidewall curvature for averaged series of **PP** and **UP** complexes. For details of the plot, see text.

acetone with carboxylic groups on the surface of SWCNTs could not explain the small irreversible shift of sensor baseline after the first pulse of acetone as reported by Snow and Robinson.[13] The baseline shift might be due to irreversible chemical interaction of acetone with defect sites.[19,20]

Our experiments suggest that annealing of carbon nanotubes to high temperatures (>900 K) leads to defect self-healing and closing of SWCNT ends. Annealing leads to decomposition of the surface oxygen functionalities that presumably stabilize the defects. This phenomenon is important for processing of carbon nanotubes for technological applications. In some cases, this nanotube closing should be avoided if availability of endohedral sites is a target factor, e.g., for hydrogen storage applications. In other cases, capped nanotubes might be useful, e.g., for fabrication of field emitters.[65,66]

5. Theoretical Results and Discussion

5.1. Comparison of DFTB-D with MP2 Energetics: Benchmark Results. The model systems employed in this benchmark study are classified as planar parallel 1 (**PP1**) and 2 (**PP2**), up-perpendicular 1 (**UP1**) and 2 (**UP2**), and down-perpendicular 1 (**DP1**) and 2 (**DP1**), where up and down refer to the position of the oxygen relative to the coronene plane assumed "underneath" the acetone molecule; "1" and "2" labels distinguish the two possible orientations of the acetone molecule relative to the hexagons two symmetry-unique C_2 axes parallel to the plane of the carbon hexagon (Figure 4).

Table 1 lists the interaction energies ΔE between acetone and coronene for the counterpoise-corrected various MP2 and DFTB-D levels of theory, as well as MP2 counterpoise correction (CP) in parentheses. CP is largest for **PP** compounds and is almost halved in **UP** and **DP** compounds, likely because of the reduced amount of orbital overlap due to geometrical reasons. As expected, CP is largest for the smallest basis set (SVP) and is reduced by about a factor of 2 going from one size of basis set to the next larger one. The most accurate CP-corrected MP2/QZVPP//MP2/SVP results are reproduced by DFTB-D within 2 kJ mol^{-1} accuracy when **UP** and **DP** geometries are reoptimized by the latter method. In case of **PP** geometries, the computed interaction energy very much depends on the position of the center of the acetone molecule relative to the coronene center. The center of mass of acetone in the case of the **PP1** complex is offset from the center of the acetone−coronene complex by 0.01 Å (MP2/SVP) and 0.77 Å (DFTB-D), while in the case of the **PP2** complex, the offsets are smaller and amount to 0.01 Å (MP2/SVP) and 0.32 Å (DFTB-D). If one additional hexagon ring is added around coronene (circumcoronene $C_{54}H_{18}$), DFTB-D interaction energies for corresponding **PP1** and **PP2** complexes are smaller and more similar with –24.9 and –24.4 kJ mol^{-1}, respectively, indicating that the influence of coronene edge hydrogen atoms provides an undesirable but unavoidable contribution to the DFTB-D stabilization energies. If averages are taken between the **PP1** and **PP2** structures, the DFTB-D average (−35.3 kJ mol^{-1}) is very close to the CP-corrected MP2/QZVPP average (−36.8 kJ mol^{-1}) with a difference less than 2 kJ mol^{-1}. However, we must stress that the best MP2 energies are probably still too high by a few kJ mol^{-1} compared to the basis set limit. Nevertheless, at all levels of theory the planar parallel structures are energetically more favorable than perpendicular complexes, of which the ones with oxygen pointing toward coronene are decidedly the least favorable. We presume that the multicenter contact favors the **PP** structures in dispersion energy more than the perpendicular structures. DFTB-D optimized structures give generally reduced intramolecular distances by about 0.1 to 0.2 Å relative to MP2/SVP, which, however, does not result in a large difference in energy, because the intermolecular potential energy surface is rather flat with respect to interatomic distances. Therefore, we conclude that the overall agreement between the computationally inexpensive DFTB-D interaction energies and the much more expensive CP-corrected MP2/QZVPP energetics is excellent, in agreement with other

Table 1. Counterpoise Corrected Interaction Energies ΔE (MP2 BSSE Counterpoise Corrections in Parentheses) [kJ mol^{-1}] and for Acetone−Coronene Complexes Shown in Figure 4. MP2 Energies Were Obtained At MP2/SVP Geometries

ΔE [kJ/mol]	MP2/SVP	MP2/TZVPP[a]	MP2/QZVPP[a]	DFTB–D[b]
PP1[c]	−23.92 (29.91)	−36.15 (12.93)	−39.38 (6.21)	−28.78
PP2[c]	−15.20 (28.36)	−31.02 (12.41)	−34.30 (5.76)	−41.90
UP1	−18.47 (16.36)	−29.65 (7.01)	−29.64 (3.24)	−27.84
UP2	−16.66 (16.51)	−27.88 (7.00)	−29.59 (3.29)	−28.56
DP1	−4.35 (15.23)	−8.91 (7.76)	−10.72 (3.84)	−9.85
DP2	−5.13 (14.31)	−8.91 (7.22)	−10.36 (3.69)	−9.86

[a] Geometry from MP2/SVP optimization. [b] Geometry optimized at DFTB-D level of theory. [c] Due to geometrical edge effects, these energies are remarkably different; see text.

(65) Khazaei, M.; Dean, K. A.; Farajian, A. A.; Kawazoe, Y. *J. Phys. Chem. C* **2007**, *111*(18), 6690–6693.
(66) Kowalska, E.; Kowalczyk, P.; Radomska, J.; Czerwosz, E.; Wronka, H.; Bystrzejewski, M. *J. Thermal Anal. Calorimetry* **2006**, *86*(1), 115–119.

benchmark studies that focused on molecule adsorption on graphitic walls.[35–37] This finding makes us confident to use DFTB-D for the estimation of interaction energies in much larger SWCNT−acetone complexes.

Regarding the physical nature of the interaction between acetone and coronene, we note that the adiabatic ionization potentials of coronene and acetone are very high, 7.29 and 9.70 eV, respectively, and the corresponding adiabatic electron affinities (EAs) are only 0.470 and 0.001 eV, respectively. No substantial charge transfer is therefore expected, and Mulliken population analysis[67,68] and Heinzmann-Ahlrichs modified atomic orbital (MAO) partial charges[69] derived from Hartree–Fock/SVP wave functions confirm essentially zero electron transfer. Charge polarization on the coronene surface amounts to at most a few hundredths of an electron per carbon atom by MAO and even less with Mulliken charge, and therefore we do not find that mirror charges are created on the graphitic surface due to the presence of the polar acetone molecule. This is equally true for the DFTB-D Mulliken charge analysis. Hence, we conclude that the interaction is almost entirely dominated by dispersion energies and can be treated reasonably well with the empirically damped $1/R^6$ London dispersion term. In **PP** compounds, C═O/coronene $\pi-\pi$ interactions are possible, which are considered a special case of dispersion interactions. The C−O bond is slightly tilted with oxygen pointing toward the coronene surface, with the shortest O−C(coronene) distances around 2.9 Å and the shortest C(central acetone carbon)−C(coronene) distances around 3.2 Å at the MP2/SVP level of theory. In case of corresponding DFTB-D geometries, the distances are slightly longer at 3.0 Å (O−C(coronene)) and 3.3 Å (C−C(coronene)). The exact values depend on the orientation of the acetone with respect to the coronene molecule. These distances are shorter than the sum of van der Waals radii and are therefore consistent with π-overlap between the C═O double bond of acetone and the π-orbitals of coronene.

5.2. DFTB-D Interaction Energies for Acetone−SWCNT Complexes. We have used the DFTB-D method to study the physisorption sites and interaction energies, ΔE, of acetone at various sites of SWCNTs, using a hydrogen-terminated, 10 Å long (11,9) SWCNT model tube as well as a hydrogen-terminated 10 Å (6,5) SWCNT model tube. The diameters for these species were found after geometry optimization to be 14.0 Å and 7.7 Å, respectively. Table 2 lists all computed DFTB-D interaction energies ΔE for optimized structures obtained in the respective endohedral and exohedral complexes for the (11,9) and (6,5) tubes.

Following our previous systematic scheme of placing acetone on coronene, we attempted to optimize, for each endohedral and exohedral acetone complex with the (11,9) SWCNT model tube, the two planar parallel as well as the four perpendicular adsorption arrangements of acetone on the central hexagon rings of the sidewall. In addition, in a nanotube, the tube axis breaks the centrosymmetry that existed in a coronene, and the alignments of acetone parallel or perpendicular to the tube directions are not equivalent. Therefore, we should formally consider 12 possible conformations. However, for the endohedral complexes with parallel axis alignment, we found that no local stable minimum of **DP** type exists with oxygen pointing toward the sidewall; optimization for these structures always resulted in parallel planar **PP** type complexes. For each acetone orientation of parallel alignment structures, only one minimum was found where the C−C−C axis of acetone was aligned closely to the tube direction, namely, in "armchair direction"; the alternative zigzag conformation does not correspond to a minimum structure in the case of parallel alignment. In the case of the much smaller (6,5) tube, we only found a single minimum associated with the endohedral complex, namely, the acetone aligned parallel to the tube direction, the **PP** structure. Similarly, we found only a single minimum with the exohedral structure, the **UP** structure.

Table 2. DFTB-D Interaction Energy ΔE and Its Components [kJ mol^{-1}] for Acetone−SWCNT Complexes[a]

	DFTB-D		DFTB only		D only	
ΔE [kJ/mol]	endo	exo	endo	exo	endo	exo
(11,9) Perpendicular to Tube Axis						
PP1	−44.38	−26.32	2.93	3.03	−47.32	−29.35
PP2	−44.95	−24.91	4.17	4.57	−49.11	−29.48
UP1	−39.45	−22.73	2.95	1.05	−42.40	−23.78
UP2	−39.86	−23.85	2.19	0.22	−42.05	−24.07
DP1	N/A	−7.67		6.76		−14.43
DP2	N/A	−8.41		6.34		−14.76
(11,9) Parallel to Tube Axis						
PP	−45.28	−26.04	0.93	4.17	−46.21	−30.21
UP	−38.82	−23.24	1.47	0.70	−40.29	−23.95
DP	−23.69	−9.31	6.64	5.29	−30.33	−14.61
(6,5) Parallel to Tube Axis						
PP	−74.35	N/A	23.80		−98.15	
UP	N/A	−24.56		−1.99		−22.57

[a] N/A means that optimization from this conformation resulted in a different confirmation (see text).

The resulting interaction energies for the (11,9) model tube can be compared with the values obtained for coronene at the DFTB-D level. In general, endohedral complexes between acetone and SWCNTs are more strongly bound than acetone−coronene, while exohedral complexes are slightly more weakly bound than acetone−coronene. The energy differences of similar structures between perpendicular or parallel alignments (such as perpendicular **PP1** and **PP2** and parallel **PP**) are small and on the order of a few kJ mol^{-1}. The order of the binding energy ΔE with respect to the position of oxygen decreases in the order: **PP**> **UP**> **DP**, with differences more pronounced for the more strongly bound endohedral complexes (46> 39> 24 kJ mol^{-1}) compared to the exohedral complexes (26> 23> 8 kJ mol^{-1}). This order is the same as found for the acetone−coronene complexes. Interestingly, the energy difference between **UP** and **DP** complexes is independent from endo- or exohedral adsorption, and is roughly 15 kJ mol^{-1} in favor of the minimum with O pointing away the carbon wall. This difference is almost the same as for coronene, where the **UP**−**DP** interaction energy gap is 18 kJ mol^{-1}.

By far the strongest interaction was found for the endohedral acetone complex with the small-diameter (6,5) tube with $\Delta E = -74.4$ kJ mol^{-1}. From the present results, we can roughly estimate the range of interaction energies; the strongest adsorption is inside small-diameter tubes with $\Delta E \sim -74$ kJ mol^{-1} for the (6,5) tube, which will reduce to $\Delta E \sim -45$ kJ mol^{-1} for the (11,9) tube and becoming slightly smaller as the tube diameter further increases. Exohedral adsorption with $\Delta E \sim -24$ kJ mol^{-1} is weaker regardless of the size of the tube. Table 2 also shows DFTB electronic energy ("DFTB-only") and dispersion energy E_{dis} ("-D-only", eq 1) contributions to the DFTB-D energy separately. This partitioning shows that the nature of the interaction is entirely due to dispersion. DFTB-D Mulliken population analysis reveals, as in the case of coronene, virtually zero intermolecular charge transfer and zero intramolecular charge polarization. The role of a strong dispersion field inside a small nanotube becomes clear in the case of the endohedral complex for the (6,5) tube, where

(67) Mulliken, R. S. *J. Chim. Phys.* **1949**, *46*, 497.
(68) Mulliken, R. S. *J. Chim. Phys.* **1949**, *46*, 675.
(69) Heinzmann, R.; Ahlrichs, R. *Theor. Chim. Acta* **1976**, *42*, 33.

the DFTB interaction without dispersion term is repulsive by 23.8 kJ mol^{-1}, while the attraction by dispersion interaction is ~100 kJ mol^{-1}. Preliminary results for acetone adsorption in groove sites suggest that ΔE may indeed follow an estimate of 1.5–1.7 times the interaction energy of exohedral sites proposed recently by Ellison et al.,[70] and suggest adsorption energies to be about 47 kJ mol^{-1}.

In Figure 5, we have plotted the averaged interaction energies ΔE for **PP** and **UP** structures as a function of sidewall curvature, measured continuously by the inverse of the tube diameter $1/d$, as we have done before in the case of covalent X-SWCNT bonding.[71] In the case of the small-diameter tube, we used the same ΔE for **PP** and **UP**, since in the endohedral compound, no such distinction can be made (Figure 5). Endohedral complexes exhibit acetone interaction with negative curvature and are therefore associated with negative values of $1/d$, while the situation in exohedral complexes corresponds to positive curvature/positive values of $1/d$. For zero curvature (infinite diameter), we tentatively used the averaged interaction energies for the coronene model system. Figure 5 clearly shows a trend in that the interaction strength of the acetone with the tube sidewall strongly depends on the sidewall curvature, and that endohedral complexes are only substantially stabilized over the normal graphite−acetone interaction when the sidewall curvature becomes very large.

Conclusions

In the course of acetone adsorption on SWCNTs studies at low temperature by TPD-MS and theoretical simulations, several important findings were made.

I. Acetone desorbs from SWCNTs giving three distinct desorption peaks:

a. A strongly bound adsorption form with a peak desorption maximum at 300 K (~75 kJ mol^{-1}) (Figure 1), assigned to adsorption in endohedral sites of small nanotubes (~7.7 Å) (Figure 5).

b. A second form of acetone adsorption with a desorption maximum at 240 K (~50 kJ mol^{-1}) (Figure 1), assigned to adsorption on endohedral sites of large nanotubes (~14 Å) (Figure 5). In the case of bundled SWCNT systems, this TPD peak can be assigned to acetone adsorption on grooves and possibly accessible interstitial channels. For SWCNT samples with a high fraction of amorphous carbon content, this peak might originate from interaction with amorphous carbon as well.

c. A third form with a desorption maximum at ~140 K (~30 kJ mol^{-1}) (Figure 1) was assigned to acetone adsorption on external walls (Figure 5) and multilayer formation. This peak was more pronounced for SWCNTs (systems with more graphitic-like structure), rather than for carbon black (disordered carbon).

II. Oxygen functionalities present on the surface of SWCNTs can block access to endohedral sites of small SWCNTs (~7.7 Å). Oxygen functionalities decompose at high temperatures (> 500 K) allowing access to endohedral sites.[53]

III. Acetone adsorbed at cryogenic temperatures desorbs as an intact molecule (Supporting Information Figure S3).

IV. Annealing to 1400 K leads to partial reblocking of endohedral sites for acetone. We assign this observation to the thermal closing of SWCNTs.[55,56]

V. Theoretical results indicate the following:

a. The nature of acetone interaction with SWCNTs is entirely due to the dispersion forces. No significant charge transfer or polarization was found.

b. Acetone orientation with oxygen pointing toward graphitic surfaces is energetically the least favorable orientation. Energetically most preferable is adsorption where the CCCO plane of acetone is parallel to the sidewall, followed by conformations where oxygen is pointing away from the sidewall.

c. A strong correlation between physisorption energy and sidewall curvature was found. Exohedral sites are slightly less favorable than acetone−graphite interactions (ΔE between 24 to 26 kJ mol^{-1}), while large-diameter nanotubes with endohedrally encapsulated acetone are somewhat more favorable with ΔE around 45 kJ mol^{-1}. The strongest interaction was obtained when placing acetone inside a small-diameter (6,5) nanotube, where we obtained a ΔE of 74 kJ mol^{-1} (Figure 5).

Acknowledgment. Financial support from DOE-UCR is acknowledged. One of the authors (S.I.) acknowledges support by the Ministry of Education, Culture, Sports, Science and Technology (MEXT) of Japan under SRPR of Nagoya University and by a special grant from JSPS in Priority Area "Molecular Theory for Real Systems". The theoretical work was in part supported by a CREST (Core Research for Evolutional Science and Technology) grant in the Area of High Performance Computing for Multiscale and Multiphysics Phenomena from the Japan Science and Technology Agency (JST). E.B. acknowledges support of a visiting fellowship from the JSPS. Authors acknowledge the help of Professor Strongin and Doug Hausner (Temple University) for XPS analysis and Professor Baran and Dr. Quan Wan (Temple University) for TGA analysis.

Supporting Information Available: Figure S1 shows results of XPS and TGA analysis that highlights the effect of air-HCl purification. The results of acetone desorption from a W-grid are shown in Figure S2: acetone physisorbs on tungsten with a desorption temperature of 140–150 K. In Figure S3: the same desorption profiles for different acetone fragments suggests that acetone desorbs as an intact molecule. Figure S4: profile of CO_2 extracted from full TPD spectra of a SWCNT sample in a range of 220–1400 K. Table S1 lists Cartesian coordinates obtained at the MP2/SVP and DFTB-D levels of theory for acetone, coronene, and the acetone-coronene complexes studied in the benchmark comparisons. This information is available free of charge via the Internet at http://pubs.acs.org.

LA800030Y

(70) Ellison, M. D.; Morris, S. T.; Sender, M. R.; Brigham, J.; Padgett, N. E. *J. Phys. Chem. C* **2007**, *2007*(49), 18127–18134.

(71) Zheng, G.; Wang, Z.; Irle, S.; Morokuma, K. *J. Am. Chem. Soc.* **2006**, *128*, 15117–15126.